PCCP

A computational study of the mechanism for the $C_6H_5 + CH_2O$ reaction†

W. S. Xia and M. C. Lin*

Department of Chemistry, Emory University, Atlanta, GA 30322, USA.
*E-mail: chemmcl@emory.edu*

The mechanism for the $C_6H_5 + CH_2O$ reaction has been investigated with hybrid density functional quantum-chemical and statistical theory calculations. The results reveal three possible reaction channels: (1) The abstraction reaction producing $C_6H_6 + HCO$; (2) addition to the C atom yielding $C_6H_5CH_2O$ and (3) addition to the O atom giving $C_6H_5OCH_2$. The barriers for these 3 reactions, calculated at the B3LYP/aug-cc-pvtz level of theory using the geometry optimized with B3LYP/cc-pvdz are 0.8, 1.4 and 9.1 kcal mol^{-1}, respectively. The $C_6H_5CH_2O$ radical can fragment to form $C_6H_5CHO + H$ with a barrier of 19.4 kcal mol^{-1}. It can also undergo isomerization reactions *via* two cyclic epoxy intermediates to give $C_6H_5OCH_2$ with a maximum barrier of 20.4 kcal mol^{-1}. Transition-state theory calculations using the predicted energy barriers and structures for the rate constants of the abstraction reaction (1) lead to very good agreement with our recently measured values, while the result of RRKM calculations for the isomerization/decomposition of $C_6H_5OCH_2$ to $C_6H_5CHO + H$ also agrees quantitatively with available experimental data.

1. Introduction

Formaldehyde and phenyl radicals may co-exist in hydrocarbon combustion under sooting conditions. The rate constant for the $C_6H_5 + CH_2O$ reaction has been measured recently in our laboratory[1] by cavity ringdown spectrometry (CRDS)[2] and by pulsed laser photolysis-mass spectrometry (PLP-MS)[3] over the temperature range 297–1083 K. The activation energy measured in the low-temperature region (297–600 K), 1.3 kcal mol^{-1}, could be attributed primarily to the direct H-abstraction reaction:

$$C_6H_5 + CH_2O \rightarrow C_6H_6 + HCO \quad (1)$$
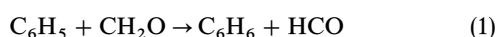
In principle, two additional reaction channels are also allowed, similar to the reaction of alkyl radicals with CH_2O:[4]

$$C_6H_5 + CH_2O \rightarrow C_6H_5CH_2O \quad (2)$$

$$C_6H_5 + CH_2O \rightarrow C_6H_5OCH_2 \quad (3)$$
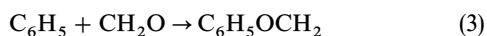
The radical adducts formed in the above addition reactions may undergo further fragmentation or isomerization reactions. The phenyl methoxy radical formed in reaction (2) can decompose rapidly to give benzaldehyde and H; whereas the phenoxy methyl radical produced in reaction (3) may undergo isomerization to phenyl methoxy as has been shown experimentally.[5,6]

The objective of this paper is to elucidate the mechanism for the $C_6H_5 + CH_2O$ reaction by fully characterizing the subsequent unimolecular reactions of the isomeric adducts using a density functional theoretical method.

II. Method of computation

The geometry of the reactants, products, van der Waals complexes, and transition states have been optimized at the hybrid density functional B3LYP method[7,8] with the correlation-consistent, polarized valence double zeta (cc-pVDZ)[9] and the polarized, triple split valence Gaussian 6-311G(d,p) basis sets.[10] Vibrational frequencies calculated at the same level of theory were employed to characterize stationary points and zero-point energy (ZPE) corrections. All the stationary points have been positively identified for local minima with the number of imaginary frequencies NIMAG = 0 and for transition states with NIMAG = 1. In order to confirm that a specific transition state connects with the designated local minima, we also performed intrinsic reaction coordinate (IRC) calculations[11] at the B3LYP/cc-pvdz and 6-311G(d,p) level of theory. To improve the energy prediction, calculations with a larger, augmented triple zeta (aug-cc-pVTZ)[9] basis set were carried out. All calculations were performed with the GAUSSIAN 94 program.[12]

III. Results and discussion

The geometries of all species have been optimized at the B3LYP/cc-pVTZ and B3LYP/6-311G(d,p) level of theory; the results are very similar and those obtained with cc-pVTZ basis set are given in Fig. 1. The predicted energies with both basis sets, summarized in Table 1, are also very close, particularly after additional single point calculations with the aug-cc-pVTZ basis set. The molecular parameters (moment of inertia and vibrational frequencies) calculated with the cc-pVDZ basis set have been provided as Electronic Supplementary Information.† The following discussions, will be based on the results of the calculations at the B3LYP/aug-cc-pVTZ// B3LYP/cc-pVDZ level of theory.

In Fig. 2, we have plotted schematically the potential energy surface (PES) profiles of the three possible reaction channels based on the predicted energies.

---

† Electronic Supplementary Information available. See http://www.rsc.org/suppdata/cp/b0/b006857h
‡ Permanent address: State Key Laboratory for Physical Chemistry of Solid Surface, Institute of Physical Chemistry and Department of Chemistry, Xiamen University, Xiamen, 361005, People's Republic of China.
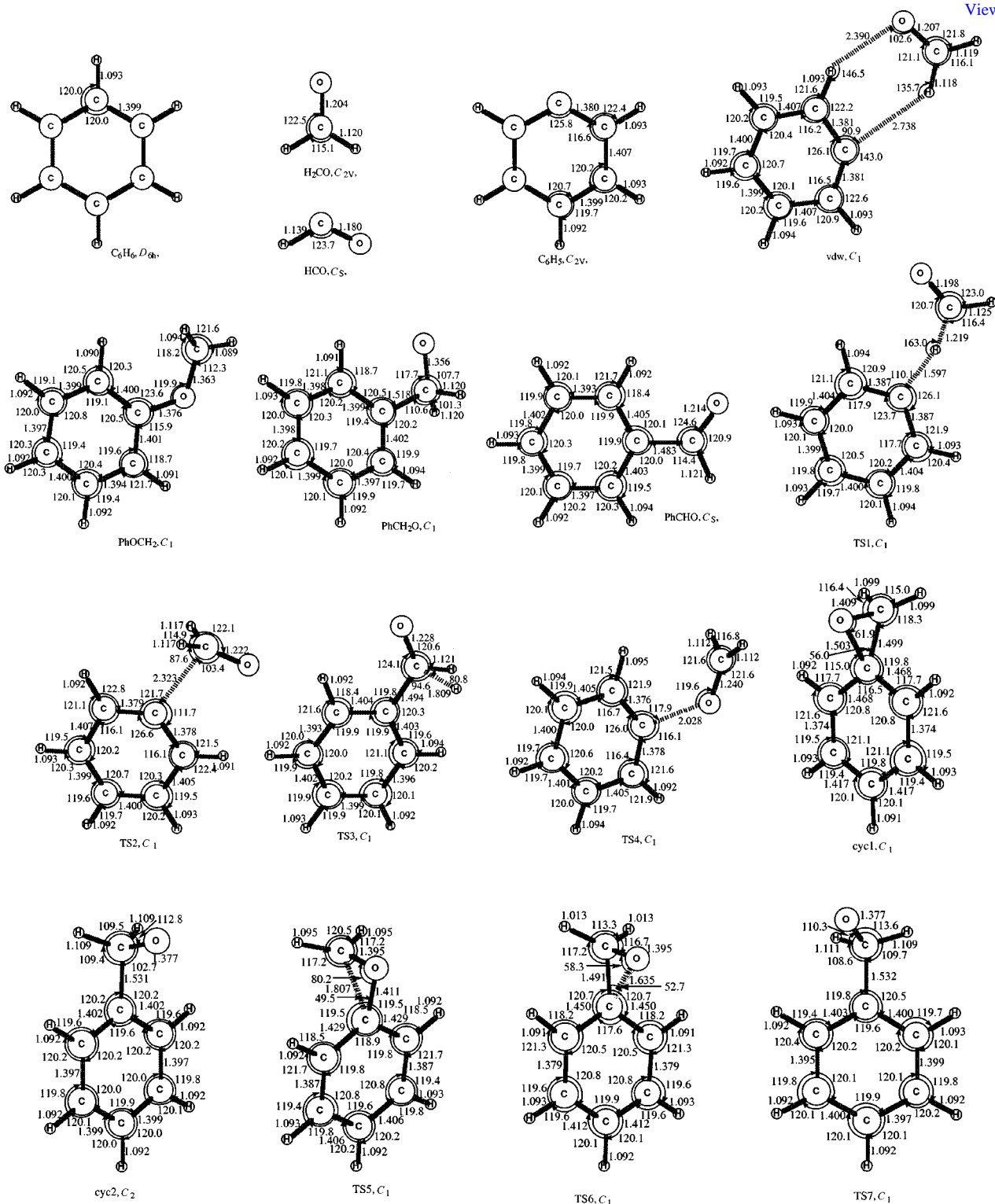
Fig. 1 Geometries of various species involved in the C_6H_5 + H_2CO reaction optimized at the B3LYP/cc-pvdz level of theory.

1. C_6H_5 + $H_2CO \rightarrow C_6H_6$ + HCO

The bimolecular abstraction reaction was found to take place *via* a van der Waals complex (vdw) $(C_5H_5)C-H-C(H)O$ with a binding energy of 0.3 kcal mol^{-1}. Geometrically, the vdw looks like a six-membered complex formed by the approaching C_6H_5 and H_2CO with a 135.7° angle for $(C_5H_5)C-H-C(H)O$. The complex goes over TS1 with a 1.1 kcal mol^{-1} activation barrier to produce C_6H_6 + HCO. At TS1, the angle of $(C_5H_5)C-H-C(H)O$ becomes 163.0°, and the forming C–H bond length, $(C_5H_5)C-HC(H)O$, is shortened to 1.597 Å from 2.738 Å in the vdw. This reaction is exother-

mic by 24.4 kcal mol^{-1}, which is in close agreement with the experimental value, 24.6 kcal mol.[13,14]

2. Formation and decomposition of $C_6H_5CH_2O$

The addition reaction *via* TS2 takes place with a 1.4 kcal mol^{-1} barrier; TS2 connects $C_6H_5CH_2O$ with the reactants. In TS2, the plane of the H_2CO moiety is almost perpendicular to the forming C···C bond with bond length 2.323 Å. The reaction is exothermic by 21.6 kcal mol^{-1}. The $C_6H_5CH_2O$ adduct can decompose to form C_6H_5CHO + H with a 19.4 kcal mol^{-1} barrier over TS3. The endothermicity of this

Table 1 Comparison of the calculated energies for various species and transition states using the B3LYP method with different basis sets. (ZPE included in all energies in units of kcal mol^{-1}; Ig: 6-311G(d,p); Ic: cc-PVDZ; IIc: aug-cc-PVTZ)

Species	Optimized at B3LYP/Ig			Optimized at B3LYP/Ic		
	ZPE	B3LYP/Ig	B3LYP/IIc	ZPE	B3LYP/Ic	B3LYP/IIc
$C_6H_5 + H_2CO$	71.2	0.0[a]	0.0[b]	71.2	0.0[c]	0.0[d]
$HCO + C_6H_6$	71.0	−24.9	−24.4	71.0	−25.2	−24.4
$C_6H_5CHO + H$	68.7	−8.4	−6.7	68.8	−10.7	−6.7
$C_6H_5CH_2O$	73.9	−23.1	−21.6	74.0	−25.1	−21.7
$C_6H_5OCH_2$	74.4	−22.9	−22.3	74.4	−25.1	−22.3
vdw	72.0	−1.8	−0.4	72.1	−2.3	−0.3
cyc1	74.2	−8.1	−8.2	74.2	−10.4	−8.2
cyc2	75.0	−19.7	−16.0	74.9	−21.2	−19.4
TS1	69.2	−0.9	0.3	69.6	−1.9	0.8
TS2	72.2	1.3	1.4	72.2	0.7	1.4
TS3	69.5	−3.3	−2.1	69.3	−5.9	−2.2
TS4	71.6	8.1	9.1	71.6	6.8	9.1
TS5	73.1	−1.5	−1.1	73.1	−3.8	−1.2
TS6	73.8	−8.1	−8.3	73.8	−10.2	−8.4
TS7	74.1	−20.4	−19.7	74.4	−21.7	−19.6

[a] −346.042 259 au. [b] −346.084 927 au. [c] −345.970 270 au. [d] −346.083 982 au.

process is 14.9 kcal mol^{-1} and the overall enthalpy change for $C_6H_5 + CH_2O \rightarrow C_6H_5CHO + H$ is predicted to be −6.7 kcal mol^{-1}, somewhat smaller than the experimental exothermicity, 11.7 kcal mol^{-1}.[13,14]

3. Formation of $C_6H_5OCH_2$

To reach $C_6H_5OCH_2$ from the reactants, TS4 with an activation barrier of 9.1 kcal mol^{-1} has to be overcome the barrier is significantly higher than those of the other two pathways. In TS4, the $(C_5H_5)C-O-CH_2$ angle is 119.6°, almost the same as that of the $C_6H_5OCH_2$ product (119.9°), and the $(C_5H_5)C-OCH_2$ and $(C_5H_5)CO-CH_2$ bond lengths are 2.028 and 1.240 Å, respectively; the corresponding bonds in the adduct are 1.376 and 1.363 Å. The enthalpy change for this reaction is −22.3 kcal mol^{-1}. No experimental data are available for comparison.

In our experimental paper,[1] we reported the kinetically measured results for the $C_6H_5 + CH_2O$ reaction by CRDS and PLP-MS at the temperatures $T = 298–1083$ K. Our results suggest that the abstraction channel (1) dominates with a small contribution from channel (2) at higher temperatures. The measured rate constant could be quantitatively accounted for by the predicted transition state energy and molecular parameters by means of a canonical variational transition-state theory (CVTST) calculation, as will be discussed later.

4. Isomerization of $C_6H_5OCH_2$ to $C_6H_5CH_2O$

As shown by the PES in Fig. 2, the enthalpy change from $C_6H_5OCH_2$ to $C_6H_5CH_2O$ is 0.7 kcal mol^{-1}; the isomerization of $C_6H_5OCH_2$ to $C_6H_5CH_2O$ involves three transition states, TS5, TS6 and TS7, with TS5 leading to cyc1 having the highest activation barrier, 21.1 kcal mol^{-1} above the phenoxy methyl radical. TS6 and TS7 have negligibly small activation barriers above cyc1 and cyc2, respectively. The reaction is, therefore, controlled by $C_6H_5OCH_2 \rightarrow$ TS5 $\rightarrow$ cyc1.
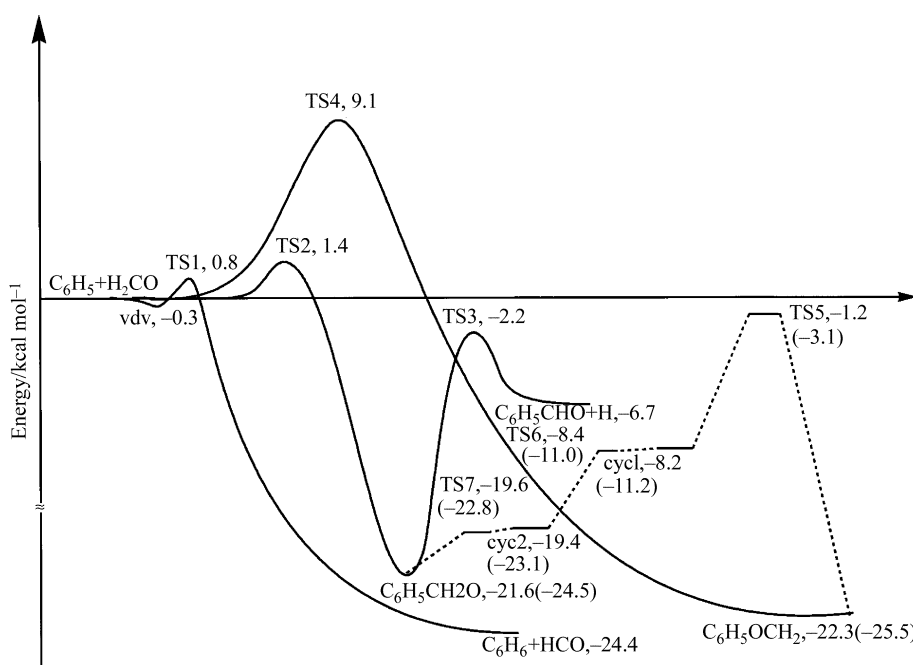
Fig. 2 PES profile of the $C_6H_5 + H_2CO$ system including the 3 separate reaction pathways (the numbers in brackets are the energies without ZPE corrections).
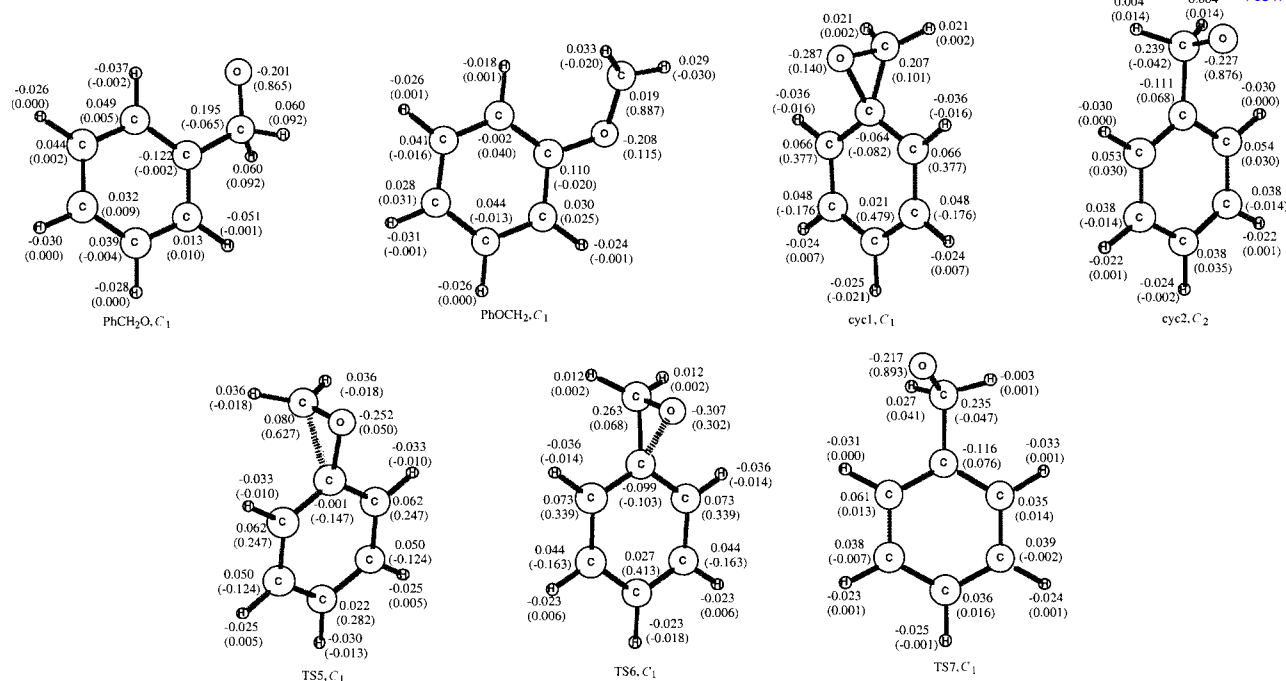
Fig. 3 Spin densities (the numbers in brackets) and charge populations for the isomers of the $C_6H_5OCH_2$ radical.

It is interesting to examine the spin densities and charge populations of various $C_6H_5OCH_2$ isomers, shown in Fig. 3. As expected, the radical site in $C_6H_5OCH_2$, based on the spin density and charge population analysis, is mostly localized at the C atom in the H_2CO moiety; whereas in cyc1 it migrates to the phenyl ring as the C atom approaches the ring and the atomic valence in the H_2CO fragment reaches saturation. For example, the spin density of the C atom in H_2CO is 0.887 in $C_6H_5OCH_2$, 0.627 in TS5, and in cyc1 it decreases to 0.207. Correspondingly, the spin density of the C atoms in the phenyl ring is increasing from $C_6H_5OCH_2$ to TS5 to cyc1. After cyc1, the radical properties move onto the O atom of the H_2CO moiety from cyc1 to TS6, to cyc2, to TS7 and finally to $C_6H_5CH_2O$, as the O atom is moving farther away from the phenyl ring. In addition, all epoxy species have a larger O atomic charge population than other non-epoxy species.

Comparing the decomposition reaction of $C_6H_5CH_2O$ with its isomerization, the PES shown in Fig. 2 indicates that decomposition barrier (19.4 kcal mol^{-1}) is far greater than the isomerization barriers to cyc2 (2.0 kcal mol^{-1}), and to cyc1 (13.2 kcal mol^{-1}). However, the tighter TS5 and its slightly higher barrier (20.4 kcal mol^{-1}) than TS3, result in a much slower rate for the isomerization than the decomposition reaction producing $C_6H_5CHO + H$.

5. Rate constant calculations

We have calculated the bimolecular rate constants for the $C_6H_5 + CH_2O \rightarrow C_6H_6 + CHO$ abstraction process as mentioned above and for the addition/decomposition and the addition/isomerization reactions. The predicted rate constants are summarized in Fig. 4 and 5. As shown in Fig. 4 for reaction (1), our recently measured total rate constant by CRDS based on the decay of C_6H_5 and that for the production of C_6H_6 (solely by the abstraction process) agrees reasonably with the predicted value by the conventional TST[15] assuming a fixed transition state (TS1) with the barrier of 0.8 kcal mol^{-1}, including Eckart-tunneling corrections, particularly at $T \leqslant 500$ K (see the dashed curve). In order to achieve a better agreement for $T > 500$ K, a CVTST calculation based on the maximum free energy criterion[16] has been made; such a calculation led to significantly better agreement at higher tem-
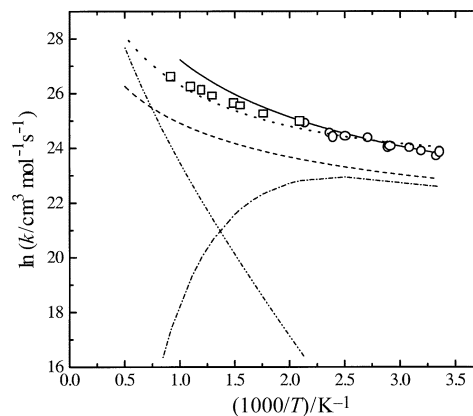

Fig. 4 Comparison of the measured rate constant by CRDS ($\bigcirc$) and PLP-MS ($\square$) with the predicted values. For reaction (1): prediction by CTST (solid curve), CVTST (dotted curve); for addition reactions by RRKM calculations on formation of $C_6H_5CHO + H$ (dashed curve), $C_6H_5CH_2O$ (dash-dotted curve) and $C_6H_5OCH_2$ (dash-double dotted curve) at 3 Torr He buffer gas (ref. 1).

peratures, with a slightly adjusted barrier from 0.8 to 1.1 kcal mol^{-1}.[1]

The result of the RRKM[15] calculations, shown in Fig. 4, for the addition/decomposition reaction producing $C_6H_5CHO + H$ or $C_6H_5CH_2O$ (by collisional stabilization) shows that the predicted rate constants cannot compete with that of reaction (1) below 1000 K because of the much tighter TS2 and TS3. Reaction (3) forming $C_6H_5OCH_2$ is even slower because of the considerably higher TS4. At temperatures above 1500 K, all 3 reaction channels become competitive; however, because of the instability of $C_6H_5OCH_2$ and $C_6H_5CH_2O$ at high temperatures, the formation of the $C_6H_5CHO + H$ products should become dominant.

Although the results obtained for these addition processes could not be tested experimentally, kinetic data exist for the isomerization of the $C_6H_5OCH_2$ radical to $C_6H_5CH_2O$ and its decomposition products, $C_6H_5CHO + H$.[5,6] In Fig. 5, we compare the predicted rate constants at 2 and 20 Torr pres-
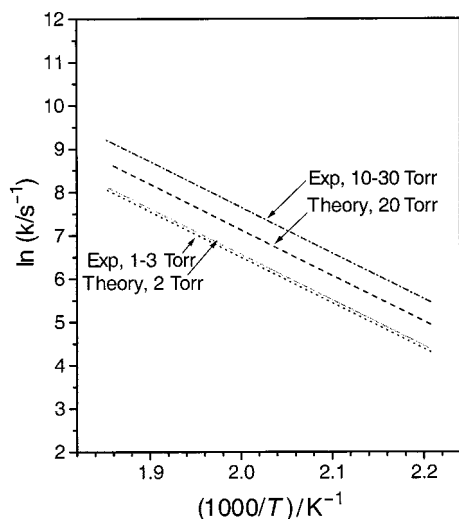
Fig. 5 Comparison of experimental rate constants with the predicted values at 2 and 20 Torr by RRKM calculations for the reaction $C_6H_5OCH_2 \rightarrow C_6H_5CHO + H$. The experimental value at 20 Torr has been adjusted as described in the text.

sures in units of s^{-1}:

$$k_{iso}(2\ \text{Torr}) = 1.07 \times 10^{12} \exp(-21.1\ \text{kcal mol}^{-1}(RT))^{-1},$$

$$k_{iso}(20\ \text{Torr}) = 1.88 \times 10^{12} \exp(-21.4\ \text{kcal mol}^{-1}(RT))^{-1},$$

with those obtained experimentally at 1–3 and 10–30 Torr, respectively:

$$k_{iso} \approx 1 \times 10^{12} \exp(-21.0\ \text{kcal mol}^{-1}(RT)^{-1})$$

$$\text{at } T = 453\text{–}450\ \text{K}, P = 1\text{–}3\ \text{Torr};[5]$$

$$k_{iso} = 3 \times 10^{12} \exp(-21.0\ \text{kcal mol}^{-1}(RT)^{-1})$$

$$\text{at } T = 453\text{–}539\ \text{K}, P = 10\text{–}30\ \text{Torr},[6]$$

based on the measured decomposition rate relative to that for the recombination reaction, $CH_3 + C_6H_5OCH_2 \rightarrow C_6H_5OCH_2CH_3$. The latter expression was obtained by assuming the recombination rate constant to be 3×10^{13} cm^3 mol^{-1} s^{-1}, independent of temperature.

If a smaller, more reasonable recombination rate constant, say, 1.3×10^{13} cm^3 mol^{-1} s^{-1}, similar to that for $C_6H_5 + CH_3 \rightarrow C_6H_5CH_3$ recently determined in our laboratory[17] is employed, the A-factor (3×10^{12} s^{-1}) given above would become 1.3×10^{12} s^{-1}. The agreement is even better (see Fig. 5).

The rate constant for the unimolecular decomposition of $C_6H_5CH_2O$ to $C_6H_5CHO + H$ in the high-pressure limit is predicted to be

$$k_{dec} = 1.27 \times 10^{13} \exp(-20.6\ \text{kcal mol}^{-1}(RT)^{-1})\ \text{s}^{-1}.$$

This result, however, differs noticeably from that estimated by Brezinsky *et al.*[18] based on assumed transition state structure, thermochemistry and reverse barrier (2 kcal mol^{-1}):

$$k_{dec} \approx 8 \times 10^{13} \exp(-17.5\ \text{kcal mol}^{-1})\ \text{s}^{-1}.$$

IV.   Conclusion

The mechanism for the $C_6H_5 + CH_2O$ reaction has been investigated by quantum-chemical calculations employing the hybrid density functional theory with Dunning's correlation-consistent basis sets, B3LYP//aug-cc-pVTZ/cc-pVDZ, for all species involved. Three product channels have been identified: the direct H-atom abstraction by C_6H_5 producing $C_6H_6 + HCO$, the addition of C_6H_5 to the C atom of CH_2O giving $C_6H_5CH_2O$ and the addition to the O atom of CH_2O

forming $C_6H_5OCH_2$. The H-abstraction reaction was predicted to be dominant with a 0.8 kcal mol^{-1} barrier. The barriers for the formation of $C_6H_5CH_2O$ and $C_6H_5OCH_2$ were predicted to be 1.4 and 9.1 kcal mol^{-1}, respectively, at the same level of theory.

The rate constants for the abstraction reaction and the isomerization of $C_6H_5OCH_2$ to $C_6H_5CH_2O$ computed with a CV TST and RRKM theory, respectively, were found to be in good agreement with available experimental data. This result suggests that for the reaction of such a large molecular size the hybrid DFT approach, computed at the B3LYP/aug-cc-pVTZ//B3LYP/cc-pVDZ level, appears to provide a reliable estimate for the energies, frequencies and molecular structures required for rate constant prediction with appropriate statistical theories over a wide range of T,P-conditions for combustion applications.

Acknowledgements

References

1   Y. M. Choi, W. S. Xia, J. Park and M. C. Lin, *J. Phys. Chem. A*, 2000, **104**, 7030.
2   J. Park and M. C. Lin, *Cavity Ringdown Spectroscopy—A New Technique for Trace Absorption Measurements*, ACS Publication Series 720, American Chemical Society, Washington, DC, 1999, ch. 13, p. 196.
3   J. Park and M. C. Lin, *Recent Research Development in Physical Chemistry*, Transworld Research Network, India, 1998, vol. 2, p. 965.
4   NIST Chemical Kinetics Database, National Institute of Science and Technology, Washington, DC, 1998 (2Q98).
5   M. F. R. Mulcahy, B. G. Tucker, D. J. Williams and J. R. Wilmshurst, *Aust. J. Chem.*, 1967, **20**, 1155.
6   M. F. R. Mulcahy, B. G. Tucker, D. J. Williams and J. R. Wilmshurst, *J. Chem. Soc., Chem. Commun.*, 1965, 609.
7   (a) A. D. Becke, *J. Chem. Phys.*, 1993, **98**, 5648; (b) A. D. Becke, *J. Chem. Phys.*, 1992, **96**, 2155; (c) A. D. Becke, *J. Chem. Phys.*, 1992, **97**, 9173.
8   C. Lee, W. Yang and R. G. Parr, *Phys. Rev. B*, 1988, **37**, 785.
9   (a) D. E. Woon and T. H. Dunning, Jr., *J. Chem. Phys.*, 1993, **98**, 1358; (b) R. A. Kendall, T. H. Dunning, Jr. and R. J. Harrison, *J. Chem. Phys.*, 1992, **96**, 6796.
10 W. Hehre, L. Radom, P. v. R. Schleyer and J. A. Pople, *Ab initio Molecular Orbital Theory*, Wiley, New York, 1986.
11 C. Gonzalez and H. B. Schlegel, *J. Chem. Phys.*, 1989, **90**, 2154.
12 M. J. Frisch, G. W. Trucks, H. B. W. Schlegel, P. M. Gill, B. G. Johnson, M. A. Robb, J. R. Cheeseman, T. Keith, G. A. Petersson, J. A. Montgomery, K. Raghavachari, M. A. Al-Laham, V. G. Zakrzewski, J. V. Ortiz, J. B. Foresman, J. Cioslowski, B. B. Stefanov, A. Nanayakkara, M. Challacombe, C. Y. Peng, P. Y. Ayala, W. Chen, M. W. Wong, J. L. Andres, E. S. Replogle, R. Gomperts, R. L. Martin, D. J. Fox, J. S. Binkley, D. J. Defrees, J. Baker, J. P. Stewart, M. Head-Gordon, C. Gonzalez and J. A. Pople, GAUSSIAN 94, Revision D.3 edn., Pittsburgh, PA, 1995.
13 *CRC Handbook of Chemistry and Physics*, ed. D. R. Lide, CRC Press, Boca Raton, FL, 1997–98, pp. 9–70.
14 *Thermodynamics of Organic Compounds in the Gas State*, ed. M. Frenkel, G. J. Kabo, K. N. Marsh, G. N. Roganov and R. C. Wilhoit, Thermodynamics Research Center, College Station, TX, 1994, vol. I and II.
15 K. J. Laidler, *Chemical Kinetics*, Harper and Row, New York, 3rd edn., 1987.
16 D. G. Truhlar, R. S. Grev and B. C. Garrett, *J. Phys. Chem.*, 1983, **87**, 3415.
17 I. V. Tokmakov, J. Park, S. Gheyas and M. C. Lin, *J. Phys. Chem. A*, 1999, **103**, 3636.
18 K. Brezinsky, T. A. Litzinger and I. Glassman, *Int. J. Chem. Kinet.*, 1984, **16**, 1053.